Observations of Particles at their Formation Sizes in Beijing, China

Rohan Jayaratne[1†], Buddhi Pushpawela[1†], Congrong He[1], Hui Li[2], Jian Gao[2*], Fahe Chai[2], Lidia Morawska[1*],

1 International Laboratory for Air Quality and Health, Queensland University of Technology, GPO Box 2434, Brisbane 4001, Australia.
2 Chinese Research Academy of Environmental Sciences, Beijing 100012, China.

Re-Revised and Submitted to

Atmospheric Chemistry and Physics

June 2017

† Joint first authors.

* Joint **c**orresponding author contact details:

Lidia Morawska

Tel: (617) 3138 2616; Fax: (617) 3138 9079

Email: l.morawska@qut.edu.au

Jian Gao

Tel: 010 84933433; Fax: 010 84915163

Email: gaojian@craes.org.cn

Abstract

New particle formation (NPF) has been observed in many highly polluted environments of South-East Asia, including Beijing, where the extent of its contribution to intense haze events is still an open question. Estimated characteristics of NPF events, such as their starting times and formation and growth rates of particles, are more accurate when the detection range of particles extends to smaller sizes. In order to understand the very first steps of particle formation, we used a neutral cluster and air ion spectrometer (NAIS) to investigate particle characteristics at sizes exactly where atmospheric nucleation and cluster activity occurs. Observations over a continuous three-month period in Beijing showed 26 NPF events. These events generally coincided with periods with relatively clean air when the wind direction was from the less-industrialized north. No NPF were observed when the daily mean $PM_{2.5}$ concentration exceeded 43 μg m^{-3}, which was the upper threshold for particle formation in Beijing. The fraction of particles that are charged in the size range 2-42 nm was normally about 15%. However, this fraction increased to 20-30% during haze events and decreased to below 10% during NPF events. With the NAIS, we determined the starting times of NPF very precisely to a greater accuracy than has been possible in Beijing before and provided a temporal distribution of NPF events with a maximum at about 8.30 am. Particle formation rates varied between 12-38 cm^{-3} s^{-1}. Particle growth rates were estimated to be in the range 0.5-9.0 nm h^{-1}. These results are more reliable than previous studies in Beijing as the measurements were conducted for the first time at the exact sizes where clusters form into particles and provide useful insight into the formation of haze events.

Keywords: New particle formation, secondary particles, nucleation, haze events

1. Introduction

Particles in the atmosphere may be classified into two types depending on their origin. Primary particles are directly emitted by a source while secondary particles are formed through a secondary process by the homogeneous condensation of gaseous precursors. This is known as new particle formation (NPF) and has been observed in many parts of the world in many different types of environments (Curtius, 2006;Kulmala et al., 2005;Kulmala et al., 2004;Zhang et al., 2011). NPF is a complicated process where molecular clusters come together to form particles at a size of about 1.6 nm (Kulmala et al., 2004). Generally, it is favoured by clean air conditions where the particle number concentration (PNC) in the atmosphere is low, resulting in a lower particle surface available for the condensation of gases, leading to an increase of the supersaturation in the air enhancing homogeneous condensation of the gaseous species (Kulmala et al., 2005;Wu et al., 2011) and, therefore, NPF is less frequent in polluted environments. However, if the gaseous precursor concentration is high enough, NPF may occur at even higher particle concentrations (Kulmala et al., 2005;Wu et al., 2011). Jayaratne et al. (2015) showed that in the relatively clean environment of Brisbane, Australia, NPF do not occur when the ambient PM_{10} concentration exceeds about 20 μg m^{-3}. However, NPF have been commonly observed in more polluted environments like Beijing (Kulmama et al., 2016) and Shanghai (Xiao et al., 2015) in China. Kulmala et al. (2017) proposed that the survival efficiency of clusters to form particles is determined by the two key parameters – condensation sink (CS) and cluster growth rate (GR). They defined a dimensionless survival parameter, P, equal to the ratio $(CS/10^{-4}\ s^{-1})/(GR/nm\ h^{-1})$ and showed that P needs to be smaller than about 50 for a notable NPF to take place. However, it was noted that NPF occurred frequently in megacities in China where the calculated P values were much higher. They hypothesized that this discrepancy may be explained if the molecular clusters were being scavenged less effectively than expected based on their collision rates with pre-existing particles or if they grew much faster in size than our current understanding allows.

78 The study of the formation and characteristics of NPF events in Beijing is important because of its
79 possible influence on severe haze episodes (Guo et al., 2014;Huang et al., 2014). Such haze events
80 not only give rise to poor visibility but are responsible for sharp increases in respiratory problems
81 amongst the large population that is exposed. In particular, Beijing experienced severe haze
82 episodes during November and December, 2015. Daily maximum $PM_{2.5}$ values in the city exceeded
83 500 μg m^{-3} on no less than six days during the month of December, prompting two official air
84 pollution 'red alerts' to be issued (Xue et al., 2016). Close examination of the haze events
85 demonstrate that they occur in cycles of a few days and generally coincide with winds blowing from
86 the more polluted regions south of the city (Guo et al., 2014;Wu et al., 2007). Particulate matter
87 concentrations are observed to drop significantly when the winds change to a northerly direction,
88 bringing cleaner air into the city, which is when NPF events generally occur (Guo et al., 2014;Huang
89 et al., 2014).
90
91 The earliest study of NPF using a TSI scanning mobility particle sizer (SMPS) in Beijing was carried out
92 by Wehner et al. (2004). They observed NPF on 25 out of 45 days of measurement, and on each of
93 these days the PNC exceeded 10^5 cm^{-3}. Subsequent studies using the SMPS were carried out by Wu
94 et al. (2007) who showed that NPFs were observed on 50%, 20%, 35% and 45% of days during the
95 spring, summer, fall and winter seasons, respectively. Yue et al. (2010) investigated 12 NPF events
96 and showed that sulfuric acid and ammonia accounted for about 45% of the growth rate, with the
97 balance being due to organic species. Guo et al. (2014) conducted a detailed analysis over a two-
98 month period during the fall of 2013 and showed that NPF events occurred in a clear periodic cycle
99 of about 4-7 days coinciding with northerly winds bringing cleaner air into the city. The average
100 $PM_{2.5}$ values when the wind was from the north and when it was from the south were 35 and 114 μg
101 m^{-3}, respectively. The average $PM_{2.5}$ (and PNC) values during and outside the NPF periods were less
102 than 50 μg m^{-3} (greater than 2 x 10^5 cm^{-3}) and several hundred μg m^{-3} (5 x 10^4 cm^{-3}), respectively.
103 Pollution also originates from within the city – from motor vehicle emissions and industrial sources.

In general, airborne gaseous pollutants in Beijing and other urban regions in China are mainly volatile organic compounds (VOC) and oxides of nitrogen (NO_x) from local transportation and sulphur dioxide (SO_2) from regional industrial sources (Wang et al., 2009;Yue et al., 2010). However, Guo et al. (2014) showed that the nucleation and growth processes occurred on a regional scale, over several hundred km, with the effect of local sources such as motor vehicle emissions being insignificant. A good summary of the studies conducted since 2004 in Beijing may be found in Zhibin et al. (2013) and Kulmama et al. (2016).

All these previous studies in Beijing have been carried out using the SMPS. The SMPS is a good tool to determine the PNC and size distribution down to a minimum particle size of about 3 nm, although the efficiency of detection falls off below about 10 nm. Thus, an event where aerosols in the size range 3-10 nm emitted on-site as primary particles or entrained from a distant location that continue to grow to larger sizes may be mistaken for particle formation at that monitoring site. The SMPS is also not able to identify the exact time period during which particle formation occurs. An instrument that can detect particles at smaller sizes is the neutral cluster and air ion spectrometer (NAIS) from Airel Ltd. The NAIS is specifically designed to monitor NPF as it can detect particles down to their actual formation sizes (Manninen et al., 2016;Manninen et al., 2009;Mirme et al., 2007). In this paper, we present the first results of using a NAIS in Beijing over the course of three months, two months with intense haze and very few NPF events, and the other including several days with NPF. We will investigate the characteristics of the NPF events and the conditions that gave rise to them. As the measurements included the sizes at which particles formed, the results provide more reliable information of such parameters as the starting times, growth rates and formation rates of particles than has been possible in the past.

2. Methods

2.1 Instrumentation

The NAIS is an improved version of the air ion spectrometer (AIS) which was developed by Airel Ltd (Mirme et al., 2007). In both instruments, the sample air is split equally into each of two separate cylindrical spectrometer columns, one of each polarity. At the inlet to each column, a unipolar corona wire diffusion charger of the same polarity as the central electrode in the column brings the particles to an equilibrium charge distribution. They are then classified by a differential mobility analyser where the outer electrodes consist of 21 insulated sections or rings, each with its own electrometer. The charged particles in the air flow are repelled by the central electrode which has a tapered cross-section and collected by the rings. The electric field between the central electrode and the rings is fixed by the voltage on the inner electrode and the gap between the inner and outer electrodes so that only particles in a given mobility range may be collected by each ring. In this way, the instrument can separate particles into 21 mobility or size bins. A refinement in the NAIS over the AIS is that it uses controlled charging to measure the total PNC in each size range in addition to the concentration of charged particles. This is done by switching the voltage off on the corona charger during one part of the measurement cycle. Thus, the NAIS can measure both charged and neutral particles separately. The mobility range of the instrument is 3.16-0.001 $cm^2 V^{-1} s^{-1}$ which corresponds to a mobility diameter range of 0.8-42 nm. However, Asmi et al. (2009), Manninen et al. (2011) and Manninen et al. (2016) have pointed out that the lowest detection limit for the NAIS in the particle mode is about 2.0 nm owing to the presence of corona-generated ions; at sizes smaller than 2.0 nm, the NAIS cannot reliably distinguish between charged and neutral particles. Therefore, Manninen et al. (2011) specified the lowest detection limit of the NAIS to be 1.6 and 1.7 nm for negative and positive ions, respectively, and 2.0 nm for neutral particles. Therefore, in this study, we will restrict our observations to the particle size range 2.0-42 nm. A good description of the detailed operation of the NAIS may be found in Manninen et al. (2016). In this study, we set the NAIS to a measurement

cycle of 5 min consisting of 2 min each for charged and neutral particles with an offset period of 1 min. Thus, a PNC and charged particle concentration reading were obtained in real time once every 5 min.

The larger size PNC was monitored with an SMPS. The instrument was set to scan up and retrace times of 120 and 15 s respectively. The aerosol and sheath flow rates were 0.3 and 3.0 lpm, respectively. Size distributions were determined in 107 bins in the size range 14 to 673 nm. A complete size distribution record was obtained every 5 min. $PM_{2.5}$ concentrations were monitored with a tapered element oscillating monitor (TEOM) and recorded as hourly average values.

2.2 Study Design

The NAIS and SMPS were set up within a room on the roof of the Chinese Research in Atmospheric and Environmental Sciences (CRAES) Building in Beiyuan, Beijing, on the 28 October 2015 and monitoring was conducted continuously until 31 January 2016. This comprised 96 days including several episodes of very high pollution or haze days when the $PM_{2.5}$ in Beijing exceeded 100-200 μg m^{-3}. Data was lost on nine days owing to various problems such as the loss of power, software malfunction and a blocked filter during a haze event. Air was sampled through a straight steel pipe of diameter 4 cm protruding vertically through the roof of the building. Meteorological parameters, including the wind speed, wind direction, air temperature and relative humidity were monitored and recorded hourly over the course of the study period.

2.3 Analysis

2.3.1 Identification of NPF events

The NAIS provided spectragrams showing the neutral and charged particle number size distributions in real time with the concentrations shown in colour contours. The neutral and charged PNCs were

also provided in real time at 5 min intervals. NPF events were identified using the method proposed by Zhang et al. (2004). We calculated the rate of change of PNC, dN/dt, where N is the number of particles in the size range 2.0 -10.0 nm. Events with N > 10,000 cm^{-3} for at least 1 hour and dN/dt >15,000 $cm^{-3}h^{-1}$ were classified as NPF events. These events generally exhibited a 'banana shape' in the spectragrams. A day on which there was at least one NPF event as defined above was termed an "NPF day". A day where the above criteria were not fulfilled were classified as a "non-event" day. A "haze day" was defined as a day when the 24-hour average $PM_{2.5}$ concentration exceeded 75 μg m^{-3} - the national air quality standard in China. A day on which there was neither NPF or haze was defined as a "normal day". NPF events are characterised by sharp increases in the intermediate size range. The starting times of an event was determined by using the time of sudden increase in PNC in the size range 2.0 – 10.0 nm.

2.3.2 Condensation sink (CS) and coagulation sink (CoagS)

The condensation sink of particles is defined as (Dal Maso et al., 2002;Dal Maso et al., 2005;Kulmala et al., 2012;Lehtinen et al., 2003;Salma et al., 2011)

$$CS = 2\,\pi\,D\,\sum_i \beta_m\,(d_{p,i}) d_{p,i} N_i \quad (1)$$

where D is the diffusion coefficient of the condensing vapour and β_m is the transition correction factor for mass flux. d_{pi} and N_i are the diameter and the number concentration of particles in the size bin i respectively. The unit of CS is s^{-1}.

It is now well established that sulfuric acid is the key precursor gas in nucleation, although low vapour pressure organics may contribute to the subsequent aerosol growth (Curtius, 2006). Sulfuric acid has a low vapour pressure which is reduced further in the presence of water. When produced

from SO_2 in the gas phase, it is easily supersaturated and begins to condense. Moreover, most of the particles in the atmosphere are in the kinetic regime (smaller than 0.01 μm)(Seinfeld and Pandis, 2006a). In this regime, condensation is directly proportional to the RMS speed of the molecules. The RMS speed is inversely proportional to the square root of the molecular weight of the molecule. Thus, a sulfuric acid molecule, with a molecular weight of 98 g mol^{-1}, has an RMS speed that is about 30% higher than a typical organic gas molecule with a molecular weight of about 200 g mol^{-1}, Thus, condensation of sulfuric acid will occur much more readily than organic molecules. Studies in Beijing have confirmed that NPF is more likely to occur in a sulfur-rich environment than in one that is sulfur-poor ((Yue et al., 2010;Guo et al., 2014;Wu et al., 2007)). Wu et al. (2007) also assumed that sulfuric acid was the main condensable vapour in determining the particle formation rates during NPF events in Beijing.

Therefore, assuming that the main condensing vapour is sulfuric acid, we estimated the diffusion coefficient for condensing vapour using the expression

$$D = 5.0032 * 10^{-6} + 1.04 * 10^{-8} T + 1.64 * 10^{-11} T^2 - 1.566 * 10^{-14} T^3 \quad (2)$$

where D has the units of $m^2\ s^{-1}$ and where the temperature T is in Kelvin (Jeong, 2009).

The transition correction factor, β_m, was calculated using the Fuchs-Sutugin expression (Fuchs and Sutugin, 1971)

$$\beta_m = \frac{Kn + 1}{1 + (\frac{4}{3\alpha} + 0.337)Kn + (\frac{4}{3\alpha})Kn^2} \quad (3)$$

where

$$Kn = \frac{2\lambda}{d_p} \quad \text{and} \quad 0 \leq \alpha \leq 1 .$$

Here, *Kn*, the Knudsen number, describes the nature of the suspending vapour relative to the particle, λ is the mean free path of a suspending vapour molecule and d_p is the diameter of the particle (Seinfeld and Pandis, 2006b). The mass accommodation coefficient (sticking coefficient) α describes the probability of a vapour molecule sticking to the surface of a particle during vapour-particle interactions (Seinfeld and Pandis, 2006b). In this study, we assumed α = 1.

The relationship between the condensation sink and coagulation sink is given by Lehtinen et al. (2007) as

$$CoagS_{d_p} = CS.\left(\frac{d_p}{0.71}\right)^m \quad (4)$$

where the exponent m varies in the range -1.75 to -1.5 with a mean value -1.7 and the value 0.71 is the diameter of a hydrated sulfuric acid molecule. The unit of CoagS is s^{-1}.

In order to calculate the CS, we used the PNC obtained from the SMPS in the 107 size bins in the range 14-673 nm and from the NAIS in 8 size bins in the range 2-14 nm. The mean temperature in Beijing during the period of observation was close to 0ºC. The value of D calculated using equation (2) at temperature T = 273 K was 0.087 cm^2 s^{-1} which is in good agreement with the values given in the literature (Brus et al. 2016;Eisele and Hanson, 2000). The values used for the exponent m was -1.7 (Dal Maso et al., 2008) and λ =108 nm (Massman, 1998).

246 **2.3.3 Particle formation rate**

247 Particle formation or nucleation occurs from thermodynamically stable clusters in the size range 1.0-
248 2.0 nm (Kulmala et al., 2007). The formation rate may be estimated from the number of particles in
249 the smallest size bin, usually 2-3 nm in the NAIS.

250 The formation rate of particles is defined as

$$J_{d_p} = \frac{dN_{d_p}}{dt} + CoagS_{d_p}.N_{d_p} + \left(\frac{GR}{\Delta d_p}\right)N_{d_p}$$

251 (5)

252 where N_{dp} is the number concentration of particles in the size range d_p and (d_p + Δd_p) respectively
253 (Kulmala et al., 2012). In this study, we used the values d_p = 2 nm and Δd_p = 1 nm, corresponding to
254 the size range 2-3 nm. $CoagS_{dp}$ represents the loss of the particles due to coagulation in the size
255 range 2-3 nm, calculated from equation (4) with d_p = 2 nm, and *GR* is the growth rate of particles.
256 The unit of formation rate is cm^{-3} s^{-1}.

257

258 **2.3.4 Particle growth rate (GR)**

259 During an NPF event, the growth rate of particles was defined by Kulmala et al. (2012) as

$$GR = \frac{dd_p}{dt} = \frac{d_{p2} - d_{p1}}{t_2 - t_1}$$

260 (6)

261 where dp_2 and dp_1 are the diameters of particles at times t_2 and t_1, respectively. This was calculated
262 by the maximum concentration method as described in Kulmala et al. (2012) by examining the time
263 of maximum PNC at each particle size during an NPF event. First, we exported the number
264 concentrations of particles obtained from the NAIS in 14 bins in the size range 2.0 – 42.0 nm. Next,

265 we selected the time of maximum concentrations during each NPF event for each particle size bin.
266 Finally, we calculated the growth rate using the slope of the best-fitted line on the graph of median
267 diameter of particle in each size bin vs. the time of maximum concentration. The unit of GR is nm h^{-1}.

268

269 **3. Results and Discussion**

270

271 **3.1 Distribution of NPF events**

272 During the entire period of measurement, the NAIS yielded 87 complete days of data, the remaining
273 9 days being affected by instrument faults, generally due to power fluctuations. November and
274 December 2015 were particularly prone to high pollution events in Beijing. The daily average $PM_{2.5}$
275 concentration exceeded the recommended maximum of 50 μg m^{-3} in Beijing on 47 days during this
276 two-month period. The maximum daily average was 448 μg m^{-3} and this occurred on 1st December.
277 Owing to the high condensation sink on polluted days, there were relatively few NPF days during
278 these two months. There was a relative improvement of air quality after 4th January and this lasted
279 until 31st January - the end of the monitoring period, during which time, the daily average exceeded
280 100 μg m^{-3} on only four days. Enhanced $PM_{2.5}$ concentrations (> 50 μg m^{-3}) were observed on 15
281 days in January. These days occurred in groups and we could identify five such distinct periods
282 during January. No NPF events were observed during these 15 days; however, several NPF events
283 were observed on the other days during the intervening periods. A summary of the observational
284 days, together with the number of days on which data were available and NPF events were
285 observed, are shown in Table 1. Column 3 shows the numbers of days on which complete 24-hour
286 data were obtained. We note that during the 56 such days between 27th October and 31st December,
287 NPF events were observed on just 10 days, whereas during the 31 days in January 2016, NPF events
288 took place on 16 days. The near equal division between NPF days and no-NPF days in January
289 provided an ideal data set to compare the parameters and conditions on these two types of days.

290 The difference between November/December and January had a clear dependence on the $PM_{2.5}$
291 concentrations. Figure 1 gives a summary of the days on which NPF events were observed.
292
293 **3.2 Relationship between NPF events and $PM_{2.5}$ concentration**
294 In Fig 2, we take a closer look at the January data, together with the respective mean daily $PM_{2.5}$
295 concentrations. It is apparent that there were five distinct groups of NPF days in January. These are
296 labelled in 2(b). In the NAIS spectragram, shown in 2(a), the 16 NPF events are clearly observed with
297 the characteristic 'banana' shapes compressed into near-vertical bands extending up from the
298 smallest sizes. The five groups from left to right consist of 5, 3, 2, 5 and 1 NPF events, respectively
299 (Figs 2(a and b)). These groups are separated by time periods when no NPFs were observed. The
300 $PM_{2.5}$ values are clearly lower on NPF days than on the other days with mean daily values of 18 μg m^{-3}
301 and 120 μg m^{-3}, respectively. A Student's t-test showed that the difference in mean daily $PM_{2.5}$
302 values between NPF days and the other days was statistically significant at the confidence level of
303 95%. The corresponding difference was even more significant when considering the entire
304 monitoring period where the mean daily values of $PM_{2.5}$ on NPF days and the other days were 21 μg
305 m^{-3} and 143 μg m^{-3}, respectively. Figure 2(c) shows the corresponding mean daily PNC. While the
306 PNC within each group showed a greater fluctuation than the $PM_{2.5}$, the PNC on NPF days was
307 significantly higher than on non-NPF days. Therefore, although the PM is higher on haze days than
308 on NPF days, the t-tests again showed that the PNC was significantly lower on haze days than on NPF
309 days. This is explicable in terms of the particle size. Particles are significantly larger on haze days
310 than on clean days when NPF events are likely to occur.
311
312 In Fig 3, we plot the daily mean PNC against the daily mean $PM_{2.5}$ for the 31 days in January. The days
313 with NPF and the days with no NPF events clearly fall into two distinct groups according to the daily
314 mean $PM_{2.5}$ values. Pre-existing particles entering the region with the winds from the south will also
315 increase the condensation sink, further reducing the likelihood of NPF.

No NPF events were observed on a day when the mean $PM_{2.5}$ value exceeded 43 μg m^{-3}. There is some minor overlap in the PNC values on the two types of days but this is primarily because they are daily averages. When we consider the average PNC values during the NPF events alone, a t-test showed that they are significantly higher than at other days and times. However, we do see that, on haze days, the daily average PNC does not exceed 8.5 x 10^4 cm^{-3}.

3.3 Relationship between NPF events and wind direction

Previous studies have shown that the wind direction played an important role in determining the $PM_{2.5}$ concentration in Beijing (Guo et al., 2014). Again, we look at the month of January, as it provided an almost equal number of NPF days and other days and was, therefore, ideal to compare the wind direction on the two types of days. Figure 4 shows the wind direction roses for both NPF days and other days during January. The frequencies are given as percentages of time when the wind was from a given direction. There is a clear difference between the two sets of days with a strong correlation between the NPF days and the wind direction. NPF events clearly occurred on days when the wind direction was predominantly from the NW, while it was more equally distributed with a greater likelihood of arriving from the S and E during the haze days when there were no NPF events. The frequencies in the sector between NW (315º) and N (0º) on NPF days and other days were 68 % and 11 %, respectively. Air from the north of Beijing is usually cleaner than that from the more industrialized south of the city (Guo et al., 2014). Clean periods are characterised by decreased condensation sinks that promote NPF. Winds from the south bring a copious supply of freshly available gaseous precursors that should give rise to particle formation. However, the absence of NPF events during these times suggests that the wind is also carrying a large supply of particles that reduce the gaseous supersaturations required for particle formation. Thus, the observed haze events are unlikely to be caused by in-situ new particle formation and more likely to be due to particles carried by the wind into the city or being prevented from escaping due to temperature inversions in the atmosphere.

342

343 **3.4 Charged particles**

344 Next, we look at the behaviour of charged particles, with particular attention to NPF events and haze
345 events. In order to compare and contrast the characteristics of these particles, we selected a period
346 of four days, comprising two haze days that were immediately followed by two NPF days. Figure 5
347 shows the time series of the concentration of total and charged particles observed over this four-day
348 period from November 30 to December 3. The upper curve represents the total PNC while the lower
349 curve gives the charged PNC. The difference between the two curves gives the neutral PNC. The
350 conditions during the two types of events could be compared during this period as intense haze was
351 observed on the first two days (Nov 30 and Dec 1) while, following a change of wind direction near
352 midnight on the 1 December, two strong NPF events took place on the next two days (Dec 2 and 3).

353 A summary of the neutral and charged PNC during the various stages over the entire period of
354 observation are presented in Table 2. Also shown are the percentage numbers of all particles that
355 were found to be charged. NPF events and NPF days are defined in section 2.3.1. A haze day was
356 defined as a day when the 24-hour average $PM_{2.5}$ concentration exceeded 75 μg m^{-3} - the national air
357 quality standard in China. A day that met neither of these criteria was defined as a 'normal day'.
358 Thus, by our ad-hoc definition, a normal day had a daily average $PM_{2.5}$ concentration in the range 43-
359 75 μg m^{-3}, since no NPF events were observed on days when the average $PM_{2.5}$ concentration was
360 greater than 43 μg m^{-3}. The duration of the various events affected the daily values while the
361 conditions during the events affected their peak number concentrations. The values shown are the
362 means of the average $PM_{2.5}$ concentrations over all the 24-hour days. The daily mean values varied
363 from day to day, especially on days with NPF events or haze events mainly due to the different
364 durations of these events. We estimated the standard deviation about these mean values to be 20%.
365 On a normal day, around 15% of the particles larger than 2 nm are charged. The fraction that is
366 charged decreases significantly during an NPF event. This is consistent with our observations in
367 Brisbane (Jayaratne et al., 2016) and may be attributed to the rapid increase in particle number and

368 the associated coagulation. On the other hand, during a haze event, the percentage of particles
369 charged increases to a value between 20% and 30%. These observations are consistent with the PNC
370 and particle sizes and the equilibrium distribution of charge on particles. NPF are characterised by
371 large numbers of small particles while the SMPS and TEOM show that haze events comprise much
372 larger particles. The amount of charge that a particle can hold and the fraction of particles that are
373 charged in equilibrium both increase with particle size, so it is not unexpected to find that a larger
374 percentage of particles are charged during the haze events.
375
376 **3.5 Particle formation times**
377 All except one of the 26 NPF events during the period of observation began between 7:30 am and
378 10:00 am. The mean time was 8:45 am. This result is in agreement with Wu et al. (2007) who, using
379 an SMPS, reported that NPF events during clean air periods in November, December and January
380 generally started between 7:00 am and 10:00 am. Figure 6 shows the temporal distribution of the
381 start times of the NPF events, classified into 30 minute bins. The most likely time for an NPF event to
382 begin was between 8:00 and 8:30 am. This time coincides with the morning rush hour traffic when
383 the production rate of gaseous precursors is generally at a maximum. Sunrise in Beijing in
384 December/January is at about 7.30 am.
385
386 Figure 7 shows the NAIS spectragram of the strong NPF event that occurred on 29th October 2015.
387 The spectragram shows a clear banana profile which levels off at about 20 nm. The PNC in this event
388 was relatively high, exceeding 1.6 x 10^5 cm^{-3} near 11:00 am. The $PM_{2.5}$ concentration remained
389 between 12 and 16 µg m^{-3} right through this event. The markers shown on this figure are the median
390 sizes of particles at each time. It can be observed in the spectragram that particle formation began
391 at around 09:00 h. However, previous studies in Beijing have not been able to measure particles
392 smaller than 3 nm. In Fig 7, if we truncate the lower particle size margin to 3 nm, the starting time of
393 the NPF event appears later than it actually is, approximately at 9:30 am. In other NPF spectragrams,

394 we see this difference being as much as 1.0 to 1.5 h depending on the initial growth rate. Thus, we
395 conclude that the starting times that we have derived (Fig 6) are more accurate than has been
396 obtained in the past. This will also affect the estimated growth rates of particles during NPF events
397 as we shall show in the next section.

398

399 **3.6 Condensation sink**

400 The condensation sinks were calculated during NPF events assuming the growth to be due to sulfuric
401 acid and using the SMPS and NAIS data and the equations given in the methods section. The mean
402 value of the condensation sink was 4.2×10^{-3} s^{-1}. This value is somewhat smaller than that reported by
403 Wu et al. (2007) (1.4×10^{-2} s^{-1}) and Wu et al. (2011) (1×10^{-2} s^{-1}) but within the range of 0 – 5×10^{-2} s^{-1}
404 reported in all NPF events between 2004 to 2008 in Beijing by Zhibin et al. (2013). The value of the
405 condensation sink during NPF events (0.004 s^{-1}) was not significantly different to the corresponding
406 average values during other times on NPF days and on normal days with no NPF (0.006 s^{-1}).
407 However, the mean condensation sink on haze days (0.060 s^{-1}) was significantly higher than both
408 these values.

409

410 **3.7 Particle formation rate**

411

412 Using our value of the CS, we calculated the mean value of the coagulation sink using equation (4)
413 for 2 nm particles during an NPF event to be 7.2×10^{-4} s^{-1}. Previous studies in Beijing have not been
414 able to determine this value at 2 nm. The value reported for 3 nm particles for NPF events in Beijing
415 by Wu et al. (2011) was 9.9×10^{-4} s^{-1}, which is close to our value at 2 nm. Using our value of the
416 coagulation sink in equation (5), we calculated the formation rate of particles in the smallest particle
417 size bin 2-3 nm. At these times, the rate of increase of particles in this size bin ranged from about
418 5.0×10^{3} to 1.5×10^{4} cm^{-3} h^{-1}. The resulting formation rates varied between 12 and 38 cm^{-3} s^{-1}, with a
419 mean of 26 cm^{-3} s^{-1}. Previous estimates in Beijing did not have the benefit of the PNC information in

the 2-3 nm size bin. Wu et al. (2007) calculated the formation rate in the wider size bin of 3-10 nm and arrived at a value in the range 3.3-81.4 cm^{-3} s^{-1} with a mean of 22.3 cm^{-3} s^{-1}. Yue et al. (2010) studied 12 NPF events in Beijing and derived a formation rate in the range 2-13 cm^{-3} s^{-1} and showed that the formation rate was directly proportional to the sulfuric acid concentration. They did not specify the size range used in this calculation but the smallest detectable particle size of the instrument used was 3 nm. These values may be compared with that found by Yu et al. (2016) in the urban atmosphere of Nanjing, China. They studied eight NPF events using a nano-condensation nucleus counter system capable of measuring particle size distributions down to 1.4 nm and estimated initial and peak particle formation rates of $2.1x10^{2}$ and $2.5x10^{3}$ cm^{-3} s^{-1}, respectively. The formation rates showed good linear correlation with a sulfuric acid proxy.

3.8 Particle growth rate

In the NPF event shown in Fig 7, the particle growth rate in the size range 2-10 nm during the entire event (between 9:00 and 11:00 am) estimated from equation (6) was 4.8 nm h^{-1}. Although the PNC reached very high values, the particles did not grow much larger than about 30 nm, suggesting that the high condensation sink was restricting the precursor gas concentration in the atmosphere. The growth rate of all the NPFs observed ranged from 0.5 to 9.0 nm h^{-1} with a mean value of 3.5 nm h^{-1}. Previous estimates of the growth rate during NPF using the SMPS have yielded mean values of 1.0 nm h^{-1} (Wehner et al., 2004) and 1.8 nm h^{-1} (Wu et al., 2007)., 2007). Zhibin et al. (2013) determined the growth rates of a number of NPFs in Beijing over a 4-year period and reported a range of 0.1 to 10 nm h^{-1} with a mean of 3.0 nm h^{-1} which is in close agreement with our value. In contrast, Yu et al (2016) reported an exceptionally high local maximum growth rate of 25 nm h^{-1} in Nanjing, China. Our values of CS and GR give a cluster survival parameter P = 12 (Kulmala et al., 2017). This value is significantly lower than the maximum value of 50 that was specified as a condition for NPF.

4 Summary and Conclusions

We monitored charged and neutral PNC over a continuous three-month period for the first time in Beijing. The results showed 26 NPF events. No NPF were observed when the daily mean $PM_{2.5}$ concentration exceeded 43 μg m^{-3}.

A summary of the main parameters determined are shown in Table 3.

This is the first study of NPF in the particle size range below 3 nm in Beijing. This enables the derivation of more relevant and accurate estimates of parameters, such as the times of formation and growth and formation rates, than has been possible before.

The results show the following features of NPF events in Beijing:

- NPF events occur during clean air episodes when the wind direction is from the north of the city.
- We have provided the first temporal distribution chart of NPF events in Beijing which shows that all but one of the 26 events began between 7:30 and 10:00 am.
- The main characteristics of the particles in the NPF events are presented in Table 3.
- The fraction of particles that are charged was normally about 15%. This fraction increased to 20-30% during haze events and decreased to below 10% during NPF events.

Acknowledgements

This project was supported by the Australia-China Centre for Air Quality Science and Management., the National Natural Science Foundation of China (Grant No 41375132, 91544226), and the Special Funds for Research on Public Welfares of the Ministry of Environmental Protection of China (201409003)

References

Asmi, E., Sipilä, M., Manninen, H., Vanhanen, J., Lehtipalo, K., Gagné, S., Neitola, K., Mirme, A., Mirme, S., and Tamm, E.: Results of the first air ion spectrometer calibration and intercomparison workshop, Atmospheric Chemistry and Physics, 9, 141-154, 2009.

Brus, D., Skrabalova, L., Herrmann, E., Olenius, T., Travnickova, T., and Merikanto, J.: Temperature-dependent diffusion coefficient of H2SO4 in air: laboratory measurements using laminar flow technique, Atmos. Chem. Phys. Discuss., 2016, 1-26, 10.5194/acp-2016-398, 2016.

Curtius, J.: Nucleation of atmospheric aerosol particles, Comptes Rendus Physique, 7, 1027-1045, 2006.

Dal Maso, M., Kulmala, M., Lehtinen, K., Mäkelä, J., Aalto, P., and O'Dowd, C.: Condensation and coagulation sinks and formation of nucleation mode particles in coastal and boreal forest boundary layers, Journal of Geophysical Research: Atmospheres, 107, 2002.

Dal Maso, M., Kulmala, M., Riipinen, I., Wagner, R., Hussein, T., Aalto, P. P., and Lehtinen, K. E.: Formation and growth of fresh atmospheric aerosols: eight years of aerosol size distribution data from SMEAR II, Hyytiala, Finland, Boreal Environment Research, 10, 323, 2005.

Dal Maso, M., Hyvärinen, A., Komppula, M., Tunved, P., KERMINEN, V., Lihavainen, H., Viisanen, Y., HANSSON, H. C., and Kulmala, M.: Annual and interannual variation in boreal forest aerosol particle number and volume concentration and their connection to particle formation, Tellus B, 60, 495-508, 2008.

Eisele, F., and Hanson, D.: First measurement of prenucleation molecular clusters, The Journal of Physical Chemistry A, 104, 830-836, 2000.

Guo, S., Hu, M., Zamora, M. L., Peng, J., Shang, D., Zheng, J., Du, Z., Wu, Z., Shao, M., and Zeng, L.: Elucidating severe urban haze formation in China, Proceedings of the National Academy of Sciences, 111, 17373-17378, 2014.

Huang, R.-J., Zhang, Y., Bozzetti, C., Ho, K.-F., Cao, J.-J., Han, Y., Daellenbach, K. R., Slowik, J. G., Platt, S. M., and Canonaco, F.: High secondary aerosol contribution to particulate pollution during haze events in China, Nature, 514, 218-222, 2014.

Jayaratne, E., Clifford, S., and Morawska, L.: Atmospheric Visibility and PM10 as Indicators of New Particle Formation in an Urban Environment, Environmental science & technology, 49, 12751-12757, 2015.

Jayaratne, E. R., Ling, X., and Morawska, L.: Charging State of Aerosols during Particle Formation Events in an Urban Environment and Its Implications for Ion-Induced Nucleation, Aerosol and Air Quality Research, 16, 348-360, 2016.

Jeong, K.: Condensation of water vapor and sulfuric acid in boiler flue gas, ProQuest, 2009.

Kulmala, M., Vehkamaki, H., Petaja, T., Dal Maso, M., Lauri, A., Kerminen, V., Birmilli, W., and McMurry, P.: Formation and Growth Rates of Ultrafine Atmospheric Particles: A Review of Observations, Journal of Aerosol Science, 35, 143-176, 2004.

Kulmala, M., Petäjä, T., Mönkkönen, P., Koponen, I., Maso, M. D., Aalto, P., Lehtinen, K., and Kerminen, V.-M.: On the growth of nucleation mode particles: source rates of condensable vapor in polluted and clean environments, Atmospheric Chemistry and Physics, 5, 409-416, 2005.

Kulmala, M., Riipinen, I., Sipilä, M., Manninen, H. E., Petäjä, T., Junninen, H., Dal Maso, M., Mordas, G., Mirme, A., and Vana, M.: Toward direct measurement of atmospheric nucleation, Science, 318, 89-92, 2007.

Kulmala, M., Petäjä, T., Nieminen, T., Sipilä, M., Manninen, H. E., Lehtipalo, K., Dal Maso, M., Aalto, P. P., Junninen, H., and Paasonen, P.: Measurement of the nucleation of atmospheric aerosol particles, Nature protocols, 7, 1651-1667, 2012.

Kulmama, M., Petäjä, T., Kerminen, V.-M., Kujansuu, J., Ruuskanen, T., Ding, A., Nie, W., Hu, M., Wang, Z., and Wu, Z.: On secondary new particle formation in China, Frontiers of Environmental Science & Engineering, 10, 1-10, 2016.

520 Kulmala, M., Kerminen, V.-M., Petäjä, T., Aijun, D., and Wang, L.: Atmospheric Gas-to-Particle
521 Conversion: why NPF events are observed in megacities?, Faraday Discussions, 2017.
522 Lehtinen, K. E., Korhonen, H., Maso, M., and Kulmala, M.: On the concept of condensation sink
523 diameter, Boreal environment research, 8, 405-412, 2003.
524 Lehtinen, K. E., Dal Maso, M., Kulmala, M., and Kerminen, V.-M.: Estimating nucleation rates from
525 apparent particle formation rates and vice versa: Revised formulation of the Kerminen–Kulmala
526 equation, J. Aerosol Sci., 38, 988-994, 2007.
527 Manninen, H., Franchin, A., Schobesberger, S., Hirsikko, A., Hakala, J., Skromulis, A., Kangasluoma, J.,
528 Ehn, M., Junninen, H., and Mirme, A.: Characterisation of corona-generated ions used in a Neutral
529 cluster and Air Ion Spectrometer (NAIS), Atmospheric Measurement Techniques, 4, 2767, 2011.
530 Manninen, H. E., Petaja, T., Asmi, E., Ripinen, I., Nieminen, T., Mikkila, J., Horrak, U., Mirme, A.,
531 Mirme, S., Laakso, L., Kerminen, V., and Kulmala, M.: Long-term field measurements of charged and
532 neutral clusters using Neutral cluster and Air Ion Spectrometer (NAIS), Boreal Environment Research,
533 14, 591-605, 2009.
534 Manninen, H. E., Mirme, S., Mirme, A., Petäjä, T., and Kulmala, M.: How to reliably detect molecular
535 clusters and nucleation mode particles with Neutral cluster and Air Ion Spectrometer (NAIS), Atmos.
536 Meas. Tech. Discuss, 2016.
537 Massman, W.: A review of the molecular diffusivities of H 2 O, CO 2, CH 4, CO, O 3, SO 2, NH 3, N 2 O,
538 NO, and NO 2 in air, O 2 and N 2 near STP, Atmos. Environ., 32, 1111-1127, 1998.
539 Mirme, A., Tamm, E., Mordas, G., Vana, M., Uin, J., Mirme, S., Bernotas, T., Laakso, L., Hirsikko, A.,
540 and Kulmala, M.: A wide-range multi-channel Air Ion Spectrometer, Boreal Environmental Research,
541 12, 247-264, 2007.
542 Salma, I., Borsós, T., Weidinger, T., Aalto, P., Hussein, T., Dal Maso, M., and Kulmala, M.: Production,
543 growth and properties of ultrafine atmospheric aerosol particles in an urban environment, Atmos.
544 Chem. Phys, 11, 1339-1353, 2011.
545 Seinfeld, J. H., and Pandis, S. N.: Atmospheric chemistry and physics. Hoboken, NJ: Wiley, 2006b.

546 Wang, M., Zhu, T., Zheng, J., Zhang, R., Zhang, S., Xie, X., Han, Y., and Li, Y.: Use of a mobile
547 laboratory to evaluate changes in on-road air pollutants during the Beijing 2008 Summer Olympics,
548 Atmospheric Chemistry and Physics, 9, 8247-8263, 2009.
549 Wehner, B., Wiedensohler, A., Tuch, T., Wu, Z., Hu, M., Slanina, J., and Kiang, C.: Variability of the
550 aerosol number size distribution in Beijing, China: New particle formation, dust storms, and high
551 continental background, Geophysical Research Letters, 31, 2004.
552 Wu, Z., Hu, M., Liu, S., Wehner, B., Bauer, S., Wiedensohler, A., Petäjä, T., Dal Maso, M., and
553 Kulmala, M.: New particle formation in Beijing, China: Statistical analysis of a 1-year data set, Journal
554 of Geophysical Research: Atmospheres, 112, 2007.
555 Wu, Z., Hu, M., Yue, D., Wehner, B., and Wiedensohler, A.: Evolution of particle number size
556 distribution in an urban atmosphere during episodes of heavy pollution and new particle formation,
557 Science China Earth Sciences, 54, 1772, 2011.
558 Xiao, S., Wang, M., Yao, L., Kulmala, M., Zhou, B., Yang, X., Chen, J., Wang, D., Fu, Q., and Worsnop,
559 D.: Strong atmospheric new particle formation in winter in urban Shanghai, China, Atmospheric
560 Chemistry and Physics, 15, 1769-1781, 2015.
561 Xue, Y., Zhou, Z., Nie, T., Pan, T., Qi, J., Nie, L., Wang, Z., Li, Y., Li, X., and Tian, H.: Exploring the
562 Severe Haze in Beijing During December, 2015: Pollution Process and Emissions Variation, Huan jing
563 ke xue= Huanjing kexue/[bian ji, Zhongguo ke xue yuan huan jing ke xue wei yuan hui" Huan jing ke
564 xue" bian ji wei yuan hui.], 37, 1593, 2016.
565 Yu, H., Zhou, L., Dai, L., Shen, W., Dai, W., Zheng, J., Ma, Y., and Chen, M.: Nucleation and growth of
566 sub-3 nm particles in the polluted urban atmosphere of a megacity in China, Atmospheric Chemistry
567 and Physics, 16, 2641-2657, 2016.
568 Yue, D., Hu, M., Zhang, R., Wang, Z., Zheng, J., Wu, Z., Wiedensohler, A., He, L., Huang, X., and Zhu,
569 T.: The roles of sulfuric acid in new particle formation and growth in the mega-city of Beijing,
570 Atmospheric Chemistry and Physics, 10, 4953-4960, 2010.

571 Zhang, Q., Stanier, C., Canagaratna, M., Jayne, J., Worsnop, D., Pandis, S., and Jiminez, J.: Insights
572 into the Chemistry of New Particle Formation and Growth Events in Pittsburgh Based on Aerosol
573 Mass Spectrometry, Environmental Science and Technology, 38, 4797-4809, 2004.
574 Zhang, R., Khalizov, A., Wang, L., Hu, M., and Xu, W.: Nucleation and growth of nanoparticles in the
575 atmosphere, Chemical Reviews, 112, 1957-2011, 2011.
576 Zhibin, W., Min, H., Zhijun, W., and Dingli, Y.: Reasearch on the Formation Mechanisms of New
577 Particles in the Atmosphere, Acta Chimica Sinica, 71, 519-527, 2013.

578

579

Figures

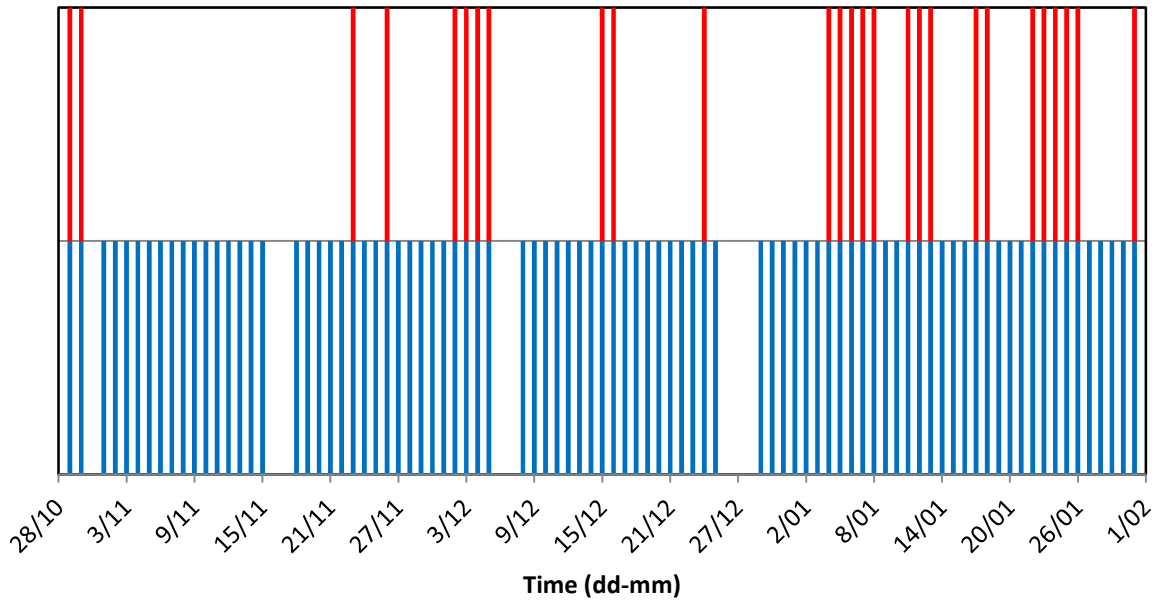

Figure 1: Summary of observational days (lower panel in blue) and days with NPF events (upper panel in red).

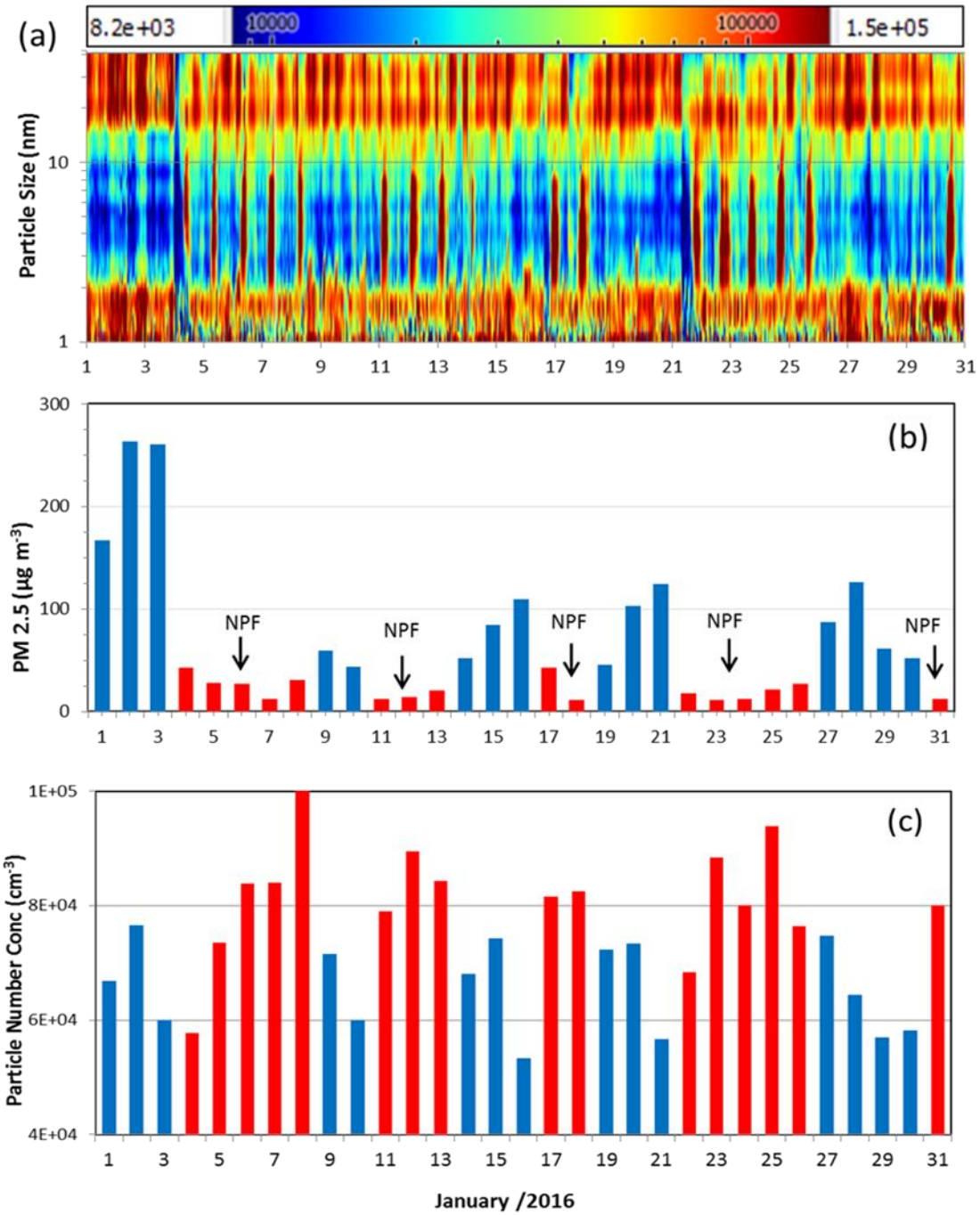

587

588

589 Figure 2: Daily values for January 2016: (a) NAIS Spectragram of PNC on a particle size–time diagram
590 (b) mean $PM_{2.5}$ concentration from the TEOM and (c) mean PNC in the size range 2 – 42 nm
591 from the NAIS. In (a), the units of PNC are cm^{-3}. Data below 2.0 nm should be treated with
592 caution due to instrumentation limitations as described in the text. In (c), the red and blue
593 bars represent the NPF days and other days, respectively.

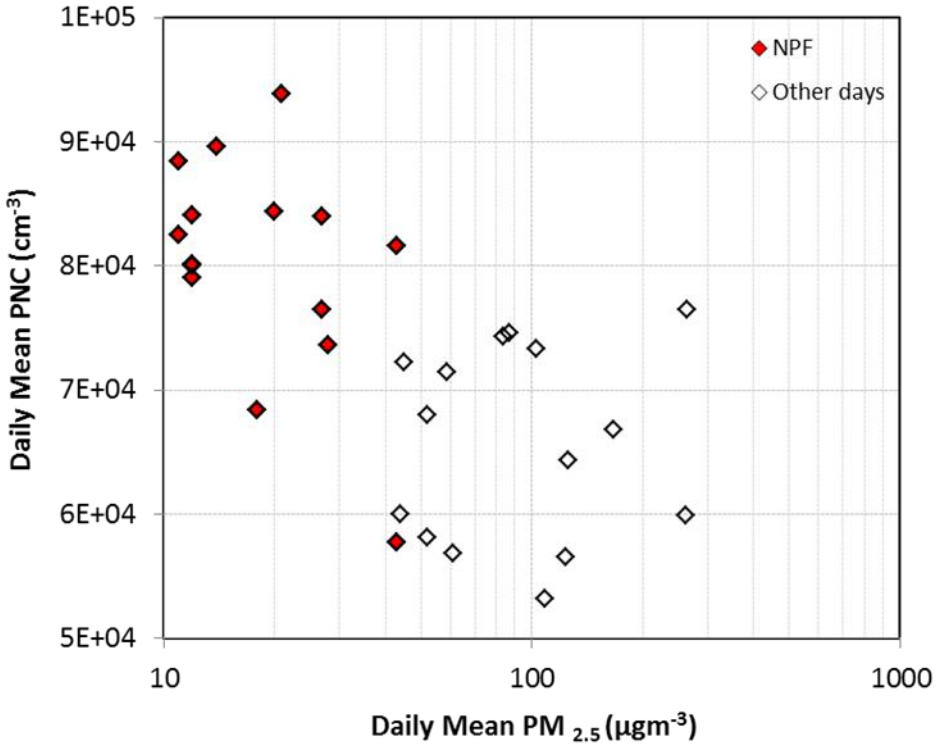

Figure 3: Daily mean PNC vs $PM_{2.5}$ for NPF days (filled markers) and other days (open markers) during January 2016.

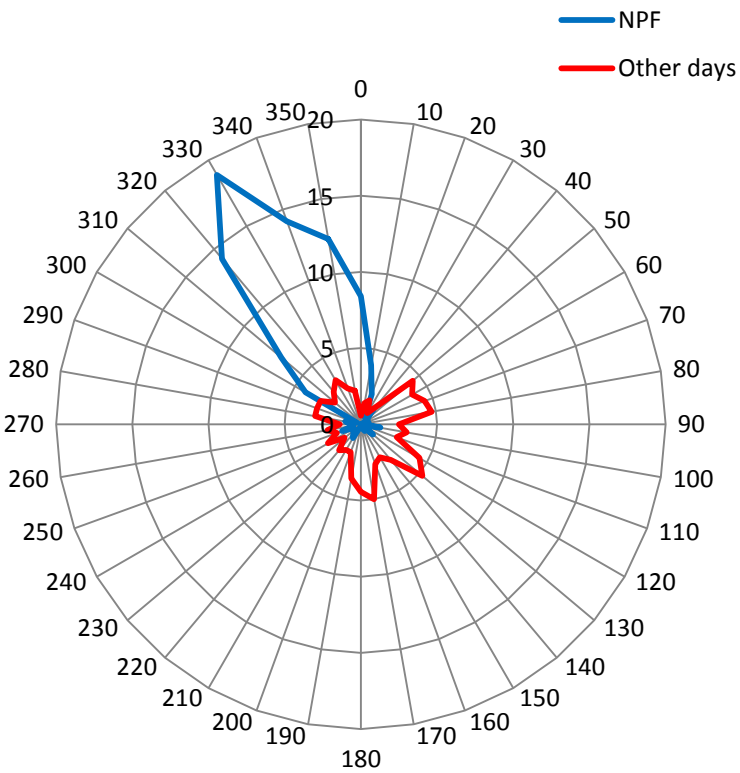

599

600

601 Figure 4: The wind direction rose for NPF days and other days during January. The radial scale

602 indicates percentages of time.

603

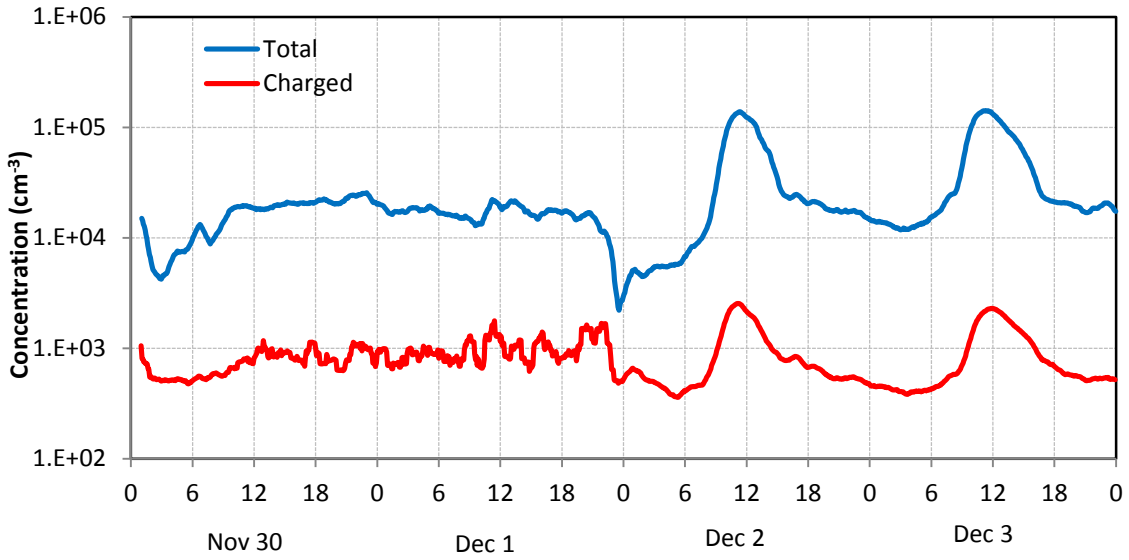

604

605

606 Figure 5: Time series of total and charged particles during the period 30 Nov to 3 Dec as measured

607 by the NAIS. 30 Nov and 1 Dec were haze days while two NPF events occurred on 2 and 3

608 Dec.

609

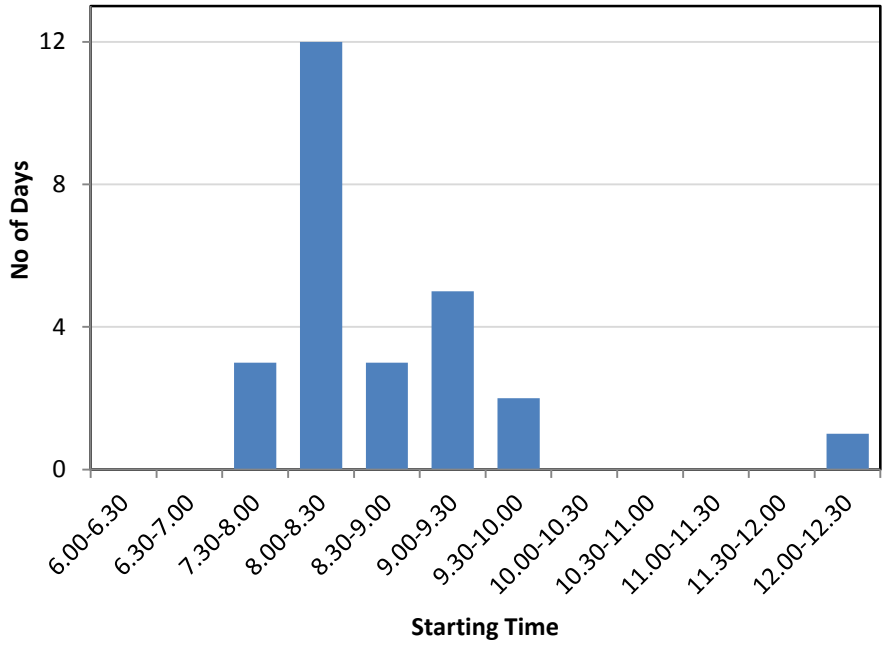

610

611 Figure 6: Distribution of the start times of the NPF events, classified into 30 min bins.

612

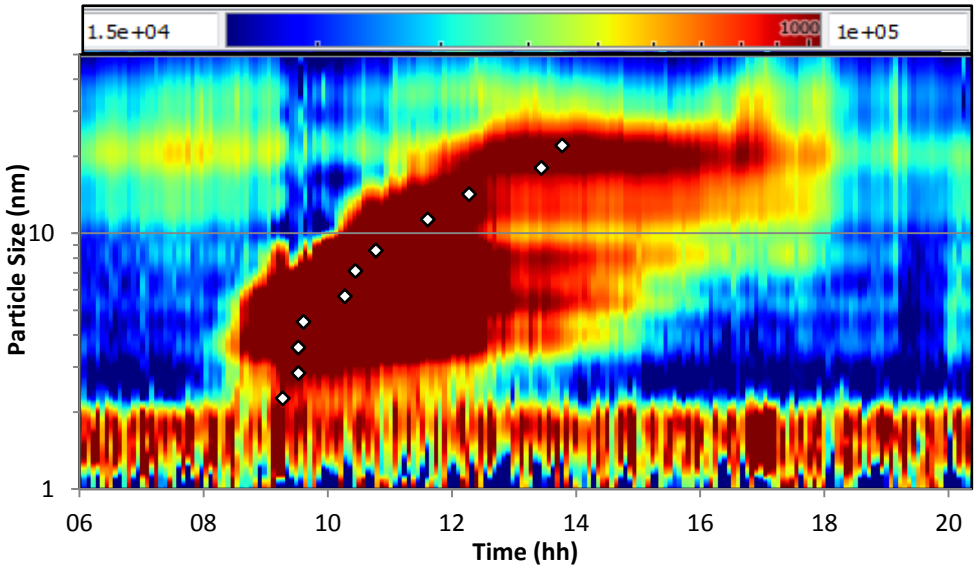

613

614 Figure 7: NAIS spectragram of the NPF event that occurred on 29th October. The clear banana shape

615 indicates strong particle growth. The markers show the median particle size at each time.

616 The units of PNC are cm^{-3}. Data below 2.0 nm should be treated with caution due to

617 instrumentation limitations as described in the text.

618

Tables

Table 1: Summary of the observational days.

Month	Total Days	Data Available Days	NPF Days : dN/dt >15000 cm^{-3} h^{-1}
October (28-31)	4	2	2
November (1-30)	30	28	2
December (1-31)	31	26	6
January (1-31)	31	31	16
Total	96	87	26

624 Table 2: Mean and peak values of neutral and charged particle concentrations during the various
625 types of days and events. The associated uncertainties in the values are up to 20%. The % column
626 shows the charged/total percentages.

627

628

	Particles (cm^{-3})		
	Neutral ($x10^4$)	Charged ($x10^4$)	%
Normal Days (mean)	5.6	0.9	14.5
NPF Days (mean)	7.6	0.8	10.1
NPF Events (peak)	22.5	1.3	5.6
Haze Days (mean)	4.8	1.9	28.6
Haze Events (peak)	11.7	2.9	20.1

629

630 Table 3: Summary of mean and range of parameters calculated for the NPF events observed.

Parameter	Mean	Range
Starting Time of NPF	8.45 am	7.30 am - 12.30 pm
Condensation sink (s^{-1})	4.2×10^{-3}	$(2.3 - 5.7) \times 10^{-3}$
Coagulation sink (s^{-1})	7.2×10^{-4}	$(3.9 - 9.7) \times 10^{-4}$
Formation rate (J_2) (cm^{-3} s^{-1})	26	12 - 38
Growth rate (nm h^{-1})	3.5	0.5 - 9.0

631